# Effects of Perinatal Asphyxia on Rat Striatal Cytoskeleton

G.E. SARACENO,[1] M.V. AYALA,[1] M.S. BADORREY,[1] M. HOLUBIEC,[1] J.I. ROMERO,[1] P. GALEANO,[1] G. BARRETO,[3] L.D. GIRALDEZ-ALVÁREZ,[4] R. KÖLLIKER-FRES,[1] H. COIRINI,[2] AND F. CAPANI[1]*

[1]*Laboratorio de Citoarquitectura y Plasticidad Neuronal, Instituto de Investigaciones cardiológicas "Prof. Dr. Alberto C. Taquini" (ININCA), Facultad de Medicina, UBA-CONICET, Marcelo T. de Alvear 2270, C1122AAJ, Buenos Aires, Argentina*

[2]*Laboratorio de Neurobiología, Instituto de Biología y Medicina Experimental-CONICET, V. de Obligado 2490, C1428ADN, Buenos Aires, Argentina*

[3]*Departamento de Nutrición y Bioquímica, Facultad de Ciencias, Pontificia Universidad Javeriana, Bogotá D.C., Colombia*

[4]*Laboratório de Neuroquímica e Biologia Celular, Instituto de Ciências da Saúde, Universidade Federal da Bahía (UFBA), Campus do Canela, 40110-100, Salvador, Bahia, Brazil*

*KEY WORDS* striatum; perinatal asphyxia; map-2; neuronal cytoskeleton; dendritic spines

*ABSTRACT* Perinatal asphyxia (PA) is a medical condition associated with a high short-term morbimortality and different long-term neurological diseases. In previous works, we have shown that neuronal and synaptic changes in rat striatum lead to ubiprotein accumulation in post-synaptic density (PSD) after six months of sub-severe PA. However, very little is known about the synaptic and related structural modifications induced by PA in young rats. In the present work, we studied neuronal cytoskeleton modifications in striatum induced by subsevere PA in 30-day-old rats. We observed a significant decrease in the number of neurons, in particular calbindin immunoreactive neurons after PA. In addition, it was also observed that actin cytoskeleton was highly modified in the PSD as well as an increment of F-actin staining by Phalloidin-alexa$^{488}$ in the striatum of PA rats. Using correlative fluorescence-electron microscopy photooxidation, we confirmed and extended confocal observations. F-actin staining augmentation was mostly related with an increment in the number of mushroom-shaped spines. Consistent with microscopic data, Western blot analysis revealed a β-actin increment in PSD in PA rats. On the other hand, MAP-2 immunostaining was decreased after PA, being NF-200 expression unmodified. Although neuronal death was observed, signs of generalized neurodegeneration were absent. Taken together these results showed early post-synaptic F-actin cytoskeleton changes induced by PA with slightly modifications in the other components of the neuronal cytoskeleton, suggesting that F-actin accumulation in the dendritic spines could be involved in the neuronal loss induced by PA. **Synapse 66:9–19, 2012.** 

## INTRODUCTION

Perinatal asphyxia (PA) is a serious obstetric complication with high mortality and morbidity rates (van Bel et al., 2008). Following PA, approximately 45% of newborns die and another 25% have permanent neurological deficits including cerebral palsy, mental retardation, developmental delay, learning disabilities, visual and hearing impairments, and different issues in school readiness (Amiel-Tison et al., 1986; Hill et al., 1981; Gunn et al., 2000; Osborne et al., 2004; Shankaran et al., 2009; Vannucci et al., 1997). Although the immature brain is relatively protected from hypoxia by adaptive mechanisms, severe insults can trigger self-sustaining damaging cascades during days or weeks, resulting in prominent injury (Capani et al, 2001b, 2009; Ferriero et al., 2004).

Brain insults can result in loss of striatal phenotypic neurons in both the adult and developing brain (Liu et al., 2009). In particular, PA has been associ-

Contract grant sponsor: UBATYC; Contract grant number: 20020090100118; Contract grant sponsor: CONICET; Contract grant number: 11420100100159.

*Correspondence to: F. Capani; Instituto de Investigaciones Cardiológicas "Prof. Dr. Alberto C. Taquini" (ININCA), UBA-CONICET, Marcelo T. de Alvear 2270, C1122AAJ, Ciudad de Buenos Aires, Argentina. E-mail: fcapani@fmed.uba.ar

Received 10 July 2011; Accepted 17 August 2011

DOI 10.1002/syn.20978

Published online 19 August 2011 in Wiley Online Library (wileyonlinelibrary.com).

ated with selective loss of various phenotypes and alteration of neurotransmitter activity (Capani et al.; 2009; Loild et al., 1994; Mallard et al., 1995). After an injury, the central nervous system (CNS) shows irreversible changes in neuronal cytoskeleton components, like neurofilaments (NF), microtubule-associated protein 2 (MAP-2), and β-actin. NF and MAP-2 are involved in the maintenance of cell shape and axonal transport (Grafstein et al., 1980; Griffin et al., 1988). Also, MAP-2 is enriched in dendritic shaft, implicating a role in the determination and stabilization of dendritic shape during neuron development. In previous works, we have shown long-term alterations after PA, including reactive astrogliosis, increased immunoreactivity for 200-kDa high-weight neurofilaments (NF-200) (Cebral et al., 2006), high levels of ubi-proteins and free ubiquitin at the postsynaptic density (PSD) in the striatum (Capani et al., 2009), phosphorylation of high and medium molecular weight neurofilaments, and MAP-2 dendritic alterations in the hippocampus (Saraceno et al., 2010). In addition, F-actin is highly concentrated in the PSD of dendritic spines (Capani et al., 2001a, 2003).

Dendritic spines have been studied for over 100 years (Ramon y Cajal, 1905). They serve as postsynaptic site for the 90% of the excitatory synapses in the CNS. Spines are principally thought to coordinate the signaling cascades that are trigged in response to presynaptic activity. The function of dendritic spines is still under intensive investigation, but they have been implicated in different mechanisms of synaptic plasticity, learning, and memory (Fukazawa et al., 2003; Ouyang et al.; 2005; Hotulainen and Hoogenraad, 2010; Morgado et al., 2011; Svitkina et al., 2011). Moreover, alterations in the morphology and function of the dendritic spines have been involved in different brain diseases such as hypoxia-ischemia, neurodegeneration, and mental retardation (Gisselsson et al., 2005, 2010; Luebke et al., 2010; Penzes et al.; 2011; Svitkina et al., 2011). Different kind of dendritic spines were described based on their shape and actin content in the adult rat brain. Mushroom-shaped spines have stalks with a clear head differentiation while stubby spines are thick and have no neck and thin spines are characterized by being long and without neck (Capani et al. 2001c). Mushroom-shaped spines show a rich F-actin cytoskeleton network (Capani et al., 2001c; Fifkova et al., 1982), suggesting a specific role of this subtype in memory formation and storage (Fukazawa et al., 2003; Ouyang et al.; 2005). Several reports support the idea that dendritic spines are the main site for damage during brain ischemia (Capani et al., 2009) and, therefore, it is reasonable to think that the neuronal cytoskeleton could be affected by PA. On this account, the aim of this study is to investigate the changes in the cytoskeleton organization after 30 days of PA in the striatum, one of the most sensitive and vulnerable brain areas in this model (Capani et al., 2009; Kirino et al., 1982; Petito et al., 1984; Saraceno et al., 2010).

## MATERIALS AND METHODS

### Animals

All procedures involving animals were approved by the Institutional Animal Care and Use Committee at the University of Buenos Aires (School of Medicine) and conducted according to the principles of the Guide for the Care and Use of Laboratory Animals (NIH Publications No. 80-23, revised 1996). Sprague-Dawley female rats in the fifteenth day of pregnancy were placed in individual cages and maintained on a 12:12 h light/dark cycle in a controlled temperature (21 ± 2°C) and humidity (65 ± 5%) environment. The animals had access to food (Purina chow) and tap water *ad libitum*. One group of animals ($n$ = 10) was used as surrogate mothers, another group ($n$ = 14) was assigned to PA procedures.

### Induction of asphyxia

Fourteen full-term pregnant rats on gestational Day 22 were anesthetized (Dorfman et al., 2006), rapidly decapitated, and the uterus horns were isolated through an abdominal incision and placed in a water bath at 37°C for 10 and 15 min (mild PA, $n$ = 6 full-term pregnant rats), and for 19 min (severe PA, $n$ = 8 full-term pregnant rats) (Bjelke et al., 1991; Capani et al., 2009; Galeano et al., 2011; Van de Berg et al., 2003). Nineteen minutes was established as the maximum time of PA because more than 20 min result in a survival rate lower than 3% (Capani et al., 2009). Following asphyxia, the uterus horns were rapidly opened, the pups were removed, the amniotic fluid was cleaned, and the pups were stimulated to breathe by performing tactile stimulation with pieces of medical wipes for a few minutes until regular breathing was established. The umbilical cord was ligated and the animals were left to recover for 1 hour under a heating lamp. When their physiological conditions improved, they were given to surrogate mothers who had delivered normally within the last 24 h. The different groups of pups were marked and mixed with the surrogate mothers' normal litters (control animals that were left undisturbed). We maintained litters of 10 pups with each surrogate mother.

### Post-asphyctic procedures

One-month-old male rats (24 per group) were used because synapses are already mature by this time (Fiala et al., 1998). Briefly, an intracardiac perfusion was performed with normal rat Ringer's at 35°C followed by fixative under deep anaesthesia (containing 50 mg/kg ketamine, 1 mg/kg rhompun, and 5 mg/kg

acetopromazine in sterile saline). For light microscopy analysis, rats were perfused with 4% formaldehyde (made fresh from paraformaldehyde) in 0.1 M phosphate buffer, pH 7.2. The brain was removed and fixed for 2 additional hours in the same solution at 4°C. For electron microscopic studies, a fixative containing 4% formaldehyde and 0.1% glutaraldehyde was employed (Capani et al., 2009). After removing the brain from the skull, it was postfixed in the same fixative during 2 h. Coronal or sagital sections (50–80 μm) were made with a Vibratome (Leica). Some of these sections were stained with cresyl violet according to the procedures described in Capani et al. (1997).

### Materials

Eosin–phalloidin and Alexa-Phalloidin$^{488}$ were purchased from Invitrogen, (cat#A12379, Carlsbad, CA). Primary antibodies were purchased from Sigma (anti-β actin cat#A5441; anti- 200 KDa NF cat#N4142; anti-MAP-2 cat#M4403; calbidin D-28 cat# C2544). Secondary antibodies against mouse and rabbit were obtained from Jackson ImmunoResearch Laboratories (West Grove, PA). Paraformaldehyde, EM grade glutaraldehyde, sodium cacodylate and Durcupan ACM resin were obtained from Electron Microscopy Sciences (Fort Washington, PA). Special welled tissue culture plates were obtained from MatTek (Ashland, MA). Materials for Western blot analysis were purchased from Sigma-Aldrich, (St. Louis, USA).

### Immunohistochemistry

Immunohistochemistry was performed on free floating sections under moderate shaking (six CTL and six 19 min PA animals). Endogenous peroxidase was quenched (3% $H_2O_2$, 30% methanol, 70% PBS 0.1 M) and nonspecific labeling was blocked using 5% normal goat serum. Sections were incubated overnight at 4°C with a mouse monoclonal anti-MAP-2 antibody (1:500; Sigma St. Louis, MO), anti-calbindin-D28 (1:10.000; Sigma, St. Louis, MO) or antihigh molecular weight neurofilament proteins (NF-200, 1:250; Sigma St. Louis, MO) overnight at 4°C. After several washes, the sections were incubated for 2 h at room temperature with the corresponding secondary antibody (Biotinylated anti-mouse IgG or anti-rabbit IgG, diluted 1:300, Vector Laboratories Inc., Burlingame, CA). Labeling was revealed using the ABC kit (Vector Laboratories Inc., Burlingame, CA). Peroxidase activity was revealed with 0.01% hydrogen peroxide, using 3, 3′-diaminobenzidine as the chromogen (DAB, Sigma). Immunostaining was absent when the first antibody was omitted. These control sections did not develop any immunohistochemical labeling. Photographs were taken in a Leitz Laborlux S microscopy. Morphometrical studies (i.e., measurement of percentage of reactive area) were performed with the NIH Image J software under blind conditions. To minimize inter-assay variations, samples from all experimental groups were processed in parallel.

### Photooxidation

Vibratome sections (six CTL and six 19 min PA animals) were washed with 50 mM glycine–PBS containing 0.5% cold water fish gelatin to block nonspecific binding. Following 30 min of washing, the sections were incubated in a solution of 0.05% of eosin–phalloidin-0.5% cold-water fish gelatin/50 mM glycine–PBS for 2 h at 4°C on a shaker (Vicking, Argentina). For light microscopy studies, phalloidin conjugated to Alexa$^{488}$ was also used for its superior fluorescent quantum yield compared to eosin. As a negative control, eosin–phalloidin was omitted. Tissue sections stained with eosin–phalloidin were mounted on glass-welled tissue culture dishes (Mat Tek Corp) pretreated with polyethylenimine. The slices were fixed again for 2–5 min with 1% glutaraldehyde in 0.1 M cacodylate buffer, rinsed in buffer for several minutes, and placed in 50 mM glycine and potassium cyanide in cacodylate buffer for an additional 5 min to reduce nonspecific staining. Photooxidation was performed on the Zeiss Axiovert described above, equipped with a 75-W xenon arc light source. The samples were immersed in a solution of 2.8 mM diaminobenzidine in 0.1 M sodium cacodylate at 4°C bubbled with pure $O_2$, final pH 7.4, and then irradiated under conventional epifluorescence using a xenon lamp. After 6–8 min a brownish reaction product began to appear instead of the fluorescence. The process was stopped by halting the excitation (Capani et al., 2001c).

### Electron microscopy procedure

Following photooxidation, tissue sections were rinsed in 0.1 M sodium cacodylate several times and incubated for 30 min with 1% osmium tetroxide in 0.1 M sodium cacodylate, pH 7.2. After several washes in double-distilled $H_2O$, the sections were dehydrated in an ascending ethanol series, and flat embedded in Durcupan ACM resin and polymerized for 24 h at 60°C. Serial thin sections (80–100 nm) were cut with Reichert Ultracut E ultramicrotome using glass knives and examined using a JEOL 100CX electron microscope at 80–100 keV. One set of thin sections was poststained with a combination of uranyl acetate and lead citrate.

### Morphometric analysis

The volume fraction of immunoreactive material for MAP-2, NF-200, and phalloidin was estimated using the point-counting method of Weibel et al. (1978) and a grid delimiting 5000 $\mu m^2$ in the dorsal striatum. A total area of 75,000 $\mu m^2$ was used in each animal for

quantification purposes. Percentage of reactive area was estimated using Image J Program (Image J 1.41o, NIH, USA). All counts were performed on coded sections. For electron microscopy analysis sampling procedures were adapted from Harris et al. (1992) and Capani et al. (2001c). For the analysis, we used all the synapses with mushroom type dendritic spines (head larger than the neck) sampled from dorsal striatum. Mushroom type dendritic spines were used because they are the only F-actin positive spines (Capani et al. 2001c). Random fields of neuropils containing at least one synapse were photographed at 10,000× magnification and analyzed at 30,000×. We analyzed 510 control spines and 1538 spines from PA rats.

### Stereological analysis of calbindin

Striatum was defined according to Paxinos and Watson (1986). Different lines were drawn to define the exact area to be quantified. Medially, a line was drawn from the dorsal tip of the left-brain side to the top of the corpus callosum. Dorsal and lateral boundaries were defined by the corpus callosum; a line drawn from the ventral tip of the lateral ventricle to the rhinal fissure was used as a ventral boundary. Laterally, a line was drawn from the ventral tip of the lateral ventricle to the corpus callosum. Anterior and posterior boundaries for the striatum were set at bregma 1.6 mm and −0.8 mm (Capani et al., 2009; Hof et al., 2000). To estimate the total number of immunoreactive (IR) calbindin neurons, every 8th section of control ($n = 6$) and 19 min PA ($n = 6$) treated animals were analyzed using optical dissector. The CAST-Grid software (Olympus, Denmark) was used for quantification. The IR neurons, which came into focus within approximately 450 μm systematically randomly spaced dissectors, were counted at a final magnification of 3600× (distance between dissectors in mutually orthogonal directions $x$ and $y$ on the sections: 250 μm). The optical dissectors had a base area of 1250 $\mu m^2$. The estimated total number of IR neurons was calculated from the number of counted neurons and the sampling probability (Schmitz et al., 2000). Sampling was optimized for prevention of type II error probability due to stereological sampling. The precision of the estimated total numbers of neurons was predicted following Hof et al. (2000) and Capani et al. (2009).

### Subcellular fractionation and preparation of PSDs

Biochemical fractionation was performed as described previously by ¿QUIÉN? et al. (2003) (CTL, $n = 6$; 19 min PA $n = 6$). Dounce homogenates (H) of the pellets in ice-cold TEVP buffer [10 mM Tris-HCl, pH 7.4, 5 mM NaF, 1 mM Na3VO4, 1 mM EDTA, and 1 mM EGTA, 1.25 μg/ml pepstatin A, 10 μg/ml leupeptin, 2.5 μg/ml aproptionin, 0.5 mM PMSF] containing 320 mM sucrose were centrifuged at 1000 × $g$ to remove nuclei and large debris (P1). The supernatant (S1) was centrifuged at 10.000 × $g$ for 10 min to obtain a crude synaptosomal fraction (P2) and subsequently was lysed hypo-osmotically and centrifuged at 45.000 × $g$ for 90 min to obtain a pellet of the synaptosomal membrane fraction (LP1). After each centrifugation the resulting pellet was rinsed briefly with ice-cold TEVP buffer before subsequent fractioning to avoid possible crossover contamination. Protein concentration was estimated by Bradford technique.

### Western blot

Western blot analysis was carried out using LP1 fractions separated on 10% SDS-PAGE. Samples containing 50 μg of protein from each groups were applied to each lane. After electrophoresis, proteins were transferred to polyvinylidene difluoride (PVDF) membrane as described previously (Dunah et al., 1996; Luo et al., 1996; Wang et al., 1995). The membranes were incubated with a primary antibody anti β-actin (Sigma, 1:1000) overnight at 4°C. Then, after appropriate washing procedures, they were incubated with horseradish peroxidase-conjugated antimouse secondary antibody for 2 h at room temperature. The blots were developed with an ECL detection kit (Amersham). The films were scanned, and the optical density of protein bands was quantified using Gel Pro Analizer software 3.1.00.00 (Media Cybernetics, USA). We used the neuron specific enolase (NSE) (Sigma, USA) and glyceraldehyde-3-phosphate dehydrogenase (GAPDH) as loading controls (Deng et al., 2007; Murphy et al., 2000; Wang et al., 2008).

### Statistical analysis

The results were expressed as the means ± SEM. Independent $t$-tests and one-way ANOVAs followed by two-tailed Bonferroni's post hoc test were carried out. A probability was considered to be significant at 5% or less. Statistical analyses were performed using the GraphPad Prism 5.03 for windows statistical package (GraphPad software, Inc, San Diego, CA).

## RESULTS

### Effect of PA time exposure on cell survival

We exposed rat pups to PA between 10 and 19 min to analyze time dependent changes in dorsal striatum. Cresyl violet staining showed nuclear condensation in 19 min PA animals (Fig. 1). To confirm the nature of these cells, we observed osmium lead stained material at electron microscopic level. Clear nuclear condensation was only observed in neurons of 30-day-old rats exposed to PA for 19 min (Fig. 2). We

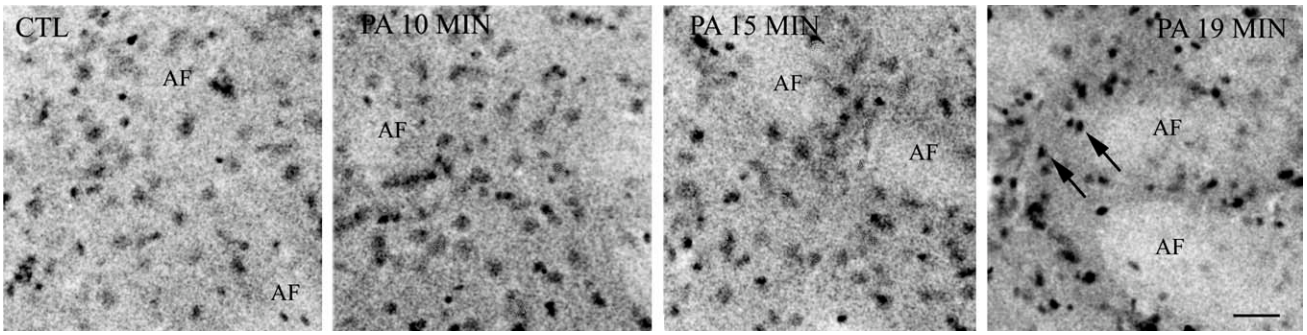


Fig. 1. Low-power micrographs of dorsal striatum from one month old CTL rats and animals subjected to different times of PA. Striatal sections were stained with cresyl violet. A clear nuclear condensation was observed after 19 min of PA (arrows). AF, axon fascicle. Scale bar, 30 μm.

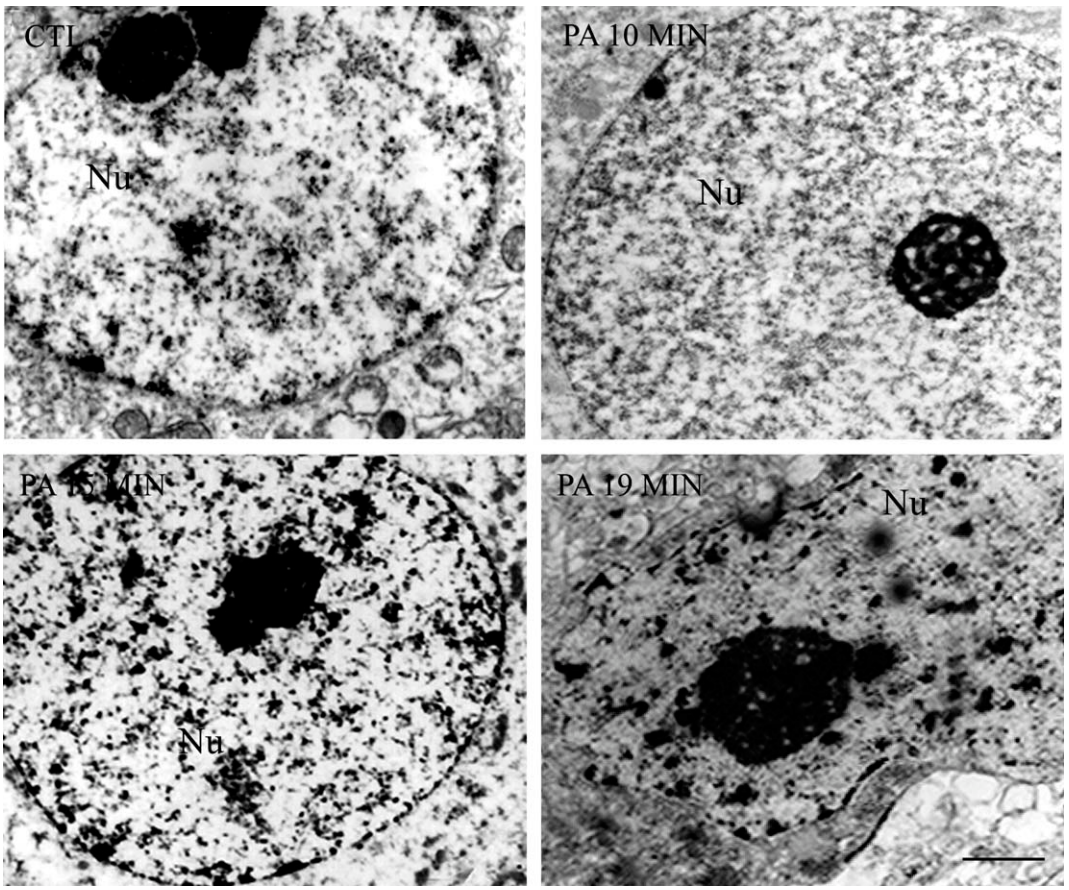


Fig. 2. Ultrastructural organization of the Golgi Type I neuron (GABAergic neuron) in the striatum area from one month old CTL rats and animals subjected to different time of PA. Note that the morphological characteristics of neurodegeneration in the 19 min PA rats are pronounced. Nu, nucleus. Scale bar, 1 μm.

also observed that most of the cells that showed nuclear condensation had morphological characteristics that correspond to neurons in degeneration, such as dark cytoplasm with vacuoles, nucleus condensation and compaction, a nucleus with a festoon shape and twisted nuclear envelope. By morphology these neurons correspond to the GABAergic Golgi type I neurons (Aggoun-Zouaoui et al., 1998; Capani et al., 1997, 2009; Liu et al., 2004). In addition, no alterations were observed in control cesarean animals (data not shown) as it was described before (Capani et al., 1997).

### Analysis of striatal GABAergic neuronal loss

Since GABAergic neurons represent the target of glutamatergic synapses from the cortex, we focused our study only on this type of neurons due to they are the principal target of anoxia in this area of the CNS (Capani et al., 2009). To quantify the loss of neurons in striatum we employed stereology combined with calbindin immunostaining that identified GABAergic neurons in striatum (Capani et al., 2009; Van de Berg et al., 2003). One-way ANOVA was significant ($F_{(3, 60)} = 9.33$, $P < 0.001$). Post hoc comparisons showed a significant decrement of the calbindin IR neurons in the 19 min PA min group in comparison with CTL group ($t = 5.050$; $df = 30$, $P = < 0.001$). The number of calbindin IR neurons from 10 and 15 min PA groups was not different from CTL group ($t = 1.436$, $df = 30$, $P =$ n.s; $t = 1.379$, $df = 30$, $P =$ n.s; respectively) (Table I). Because of the fact that 19 min of PA showed the greatest neuronal damage, we proceeded to study whether 19 min of PA induced alterations in neuronal cytoskeleton.

*TABLE 1. Estimates of the mean total number of calbindin-immunoreactive in the neostriatum*

| Groups | Means calbindin IR neurons | Cell loss |
|---|---|---|
| Control | 713.32 ± 89.39 | — |
| PA 10 min | 662.12 ± 85.26 | −9.2.0% |
| PA 15 min | 664.13 ± 119.5 | −9.3.0% |
| PA 19 min | 533.23 ± 105.6* | −25.3% |

Data are expressed as means ± SD. Each experimental group was compared to the control group (see text for statistical details).
*$P < 0.05$.

### F-actin staining in striatal dendritic spines

Punctate staining, representative of areas rich in dendritic spines, was observed at confocal level using Phalloidin-Alexa$^{488}$. An increment in the punctate staining was observed after 19 min of PA. Dendritic spines of animals subjected to 19 min of PA showed a significant increment in the reactive area stained with phalloidin ($t = 3.463$, $df = 46$; $P < 0.01$) in comparison with the control group (Fig. 3, top). The

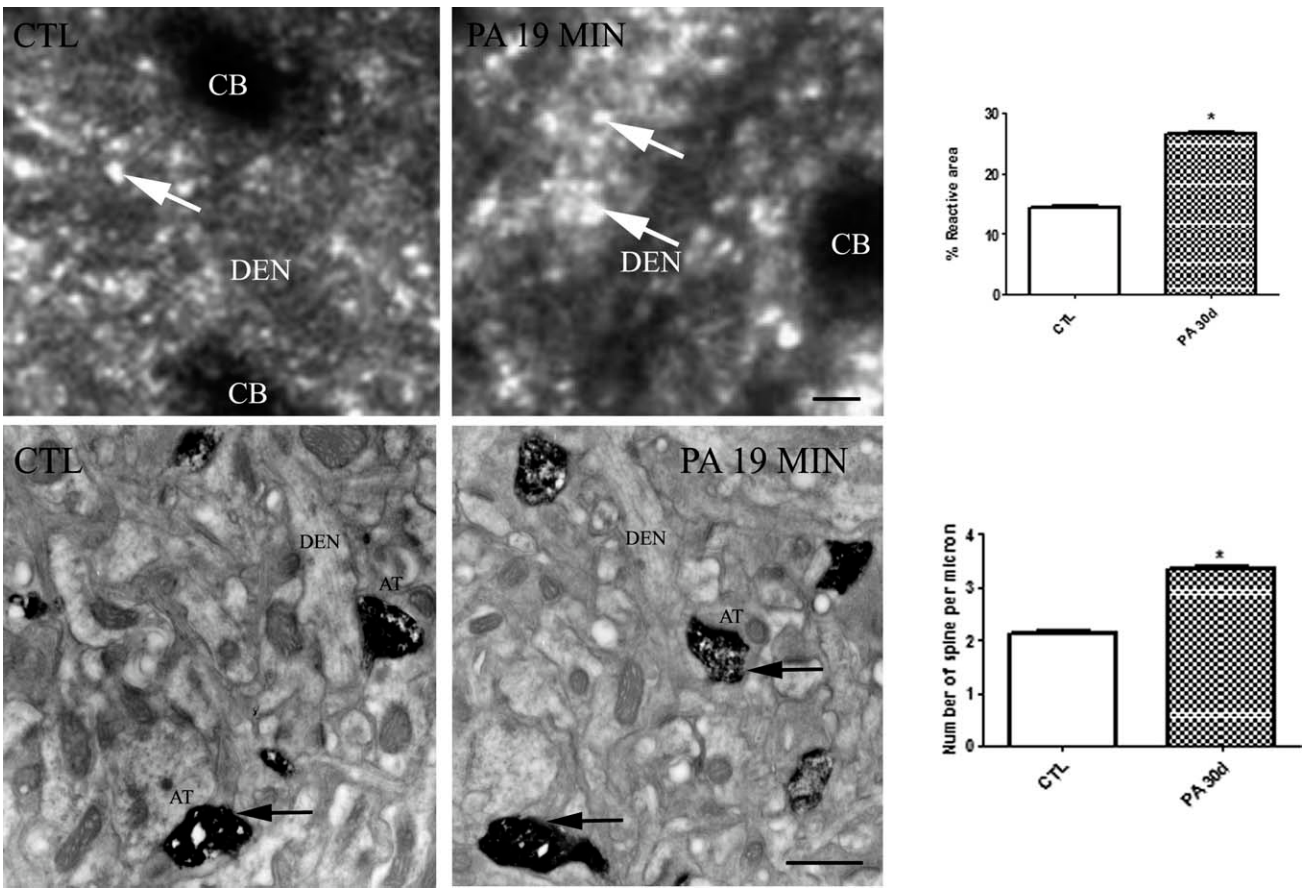


Fig. 3. Top: confocal microscope images of Phalloidin-Alexa$^{488}$ from striatum area from one month old control and asphyctic rats. An increase in the punctate staining was observed after 19 min of PA (arrows). The assessment of the percentage of the reactive area from striatal phalloidin-Alexa$^{488}$ staining in PA rats showed an increment in the reactivity area staining with phalloidin. *$P < 0.01$ Bars and error bars represent mean + SEM. DEN, dendrites; CB, cell body. Scale bar: 10 μm. Bottom: electron micrograph of photo-oxidated area in the striatum of one month old rat Arrows point out the dendritic spines stained. An increment in the number of the F-actin positive spines was observed after 19 min of PA. AT, Axon terminal; DEN, dendritic shaft. Scale bar: 1 μm. The graph shows the assessment of the number of spines per field from striatal slices. A significant increment in the number of positive F-actin spines was observed in the PA group in comparison with the CTL group. *$P < 0.01$. Bars and error bars represent mean + SEM.

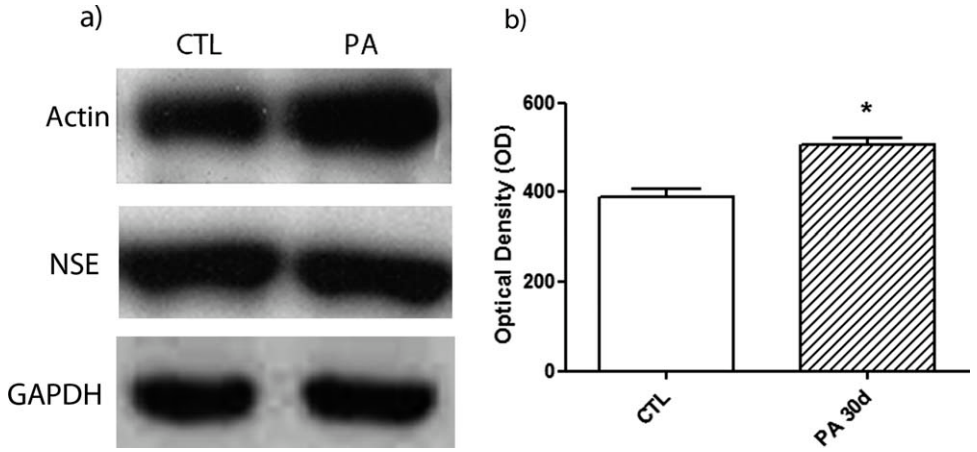


Fig. 4. Immunoblots of striatal PSDs of one-month-old CTL and PA rats. The molecular size is indicated at the left. β-actin is increased after PA. We used the neuron-specific enolase (NSE) and glyceraldehyde-3-phosphate dehydrogenase (GAPDH) as loading controls. The assessment of the percentage of optical density of PSD immunoblot bands from the one-month-old CTL and PA rats showed a significant increment in the optical density respect to control group (CTL). *$P < 0.01$. Bars and error bars represent mean + SEM. PSDs, postsynaptic densities.

morphometric analysis confirmed this data (Fig. 3, top). We and others have used correlative light and electron microscopy with phalloidin-eosin in several different studies (Capani et al., 2001a; Fukazawa et al., 2003; Ouyang et al., 2005). This technique allowed us to study F-actin changes in the different populations of dendritic spines. The analyses of spines populations in the photooxidated samples at electron microscopic level confirmed the confocal microscope observations. An increment in the number of the F-actin positive spines was observed after 19 min of PA (Fig. 3, bottom). When we analyzed the different populations of dendritic spines, we observed that only mushroom spines were the F-actin positive spines showing a significant increment in their number after 19 min of PA ($t = 22.45$, $df = 1080$, $P < 0.001$) (Fig. 3, bottom). Using conventional electron microscopic technique, we did not observe any sign of synapse degeneration at either time of asphyxia, in agreement with previous reports (Capani et al., 2009; Martone et al., 1999) (data not shown).

### Western blot analysis of the PSD fraction

To confirm the light and electron microscopic data, isolated PSD fractions were analyzed by immunoblotting with anti-β actin antibody and quantified (Fig. 4). Optical densities from the 19 min PA group were significantly higher than that of the control group ($t = 2.774$, $df = 66$, $P < 0.01$) (Fig. 4). Western blot analysis strongly supported the observations made at light and electron microscopic levels.

### Effects of PA on axon neurofilament organization

We previously reported differences in the percentage of reactive area of 200 KDa high weigh neurofilaments (NF-200) after six months of PA (Cebral et al., 2006). We performed an immunostaining of NF H in the striatum to elucidate if neurites were affected by PA (Fig. 5). In spite of observing a slight increment in the NF H immunostaining in the PA group, statistical analysis did not support this observation ($t = 1.658$; $df = 78$, $P$ = n.s) (Fig. 5).

### PA induced alterations in MAP-2 dendrites

To determine if dendritic shafts were affected by PA, an immunostaining with MAP-2 was done. In both groups, any morphological alterations were observed. Statistical analysis showed a significant decrease in MAP-2 staining in the PA group, in comparison with the control group ($t = 2.412$, $df = 74$, $P < 0.05$) (Fig. 6).

## DISCUSSION

In this study, we demonstrate that PA induces neuronal loss after one month of the injury, being the GABAergic neurons the most affected. GABAergic neuronal loss was associated with actin changes in the dendritic spines together with weak alterations in the MAP-2 dendritic shaft immunostaining. In addition no modifications in the axonal NF-H immunostaining were observed.

### GABAergic neurons are vulnerable to PA

Certain neuron subpopulations are known to be a specific target after a hypoxic-ischemic insult (Battier et al., 1998; Bottiger et al., 1998; Lap took et al., 1994; Thompson et al., 1995). This phenomenon, referred to as selective vulnerability, occurs in adult and neonatal brain. Neurons in the hippocampus, cerebellum, striatum, and neocortex are selectively

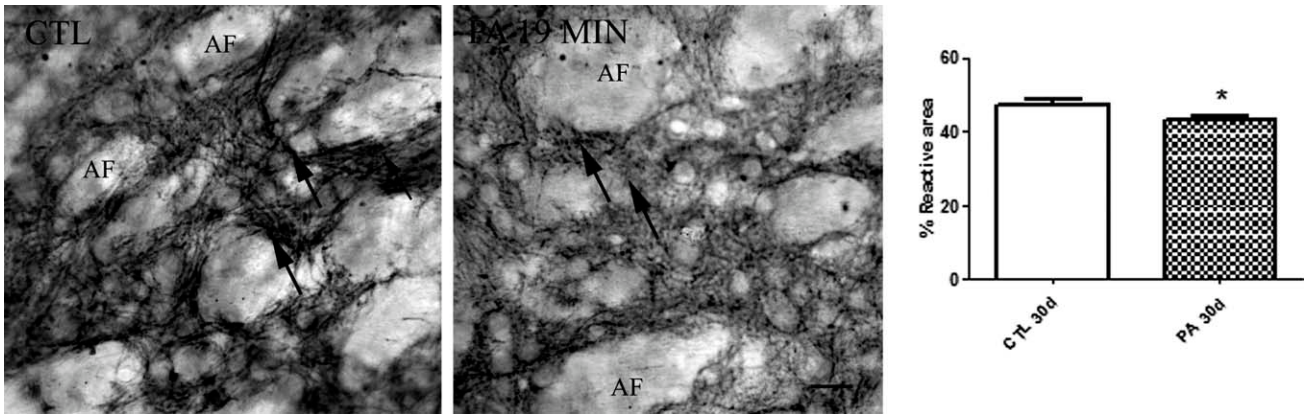


Fig. 5. Images of optical microscopy show a representative example of a striatal area immunostained for NF-200. Scale bar: 10 μm. No morphological changes were observed in PA animals respect to CTL. The statistical analysis of the percentage of reactive area of medium molecular weight neurofilaments (NF-200) did not show any difference between PA and CTL groups. AX, axon fascicles. *$P < 0.05$. Bars and error bars represent mean + SEM.

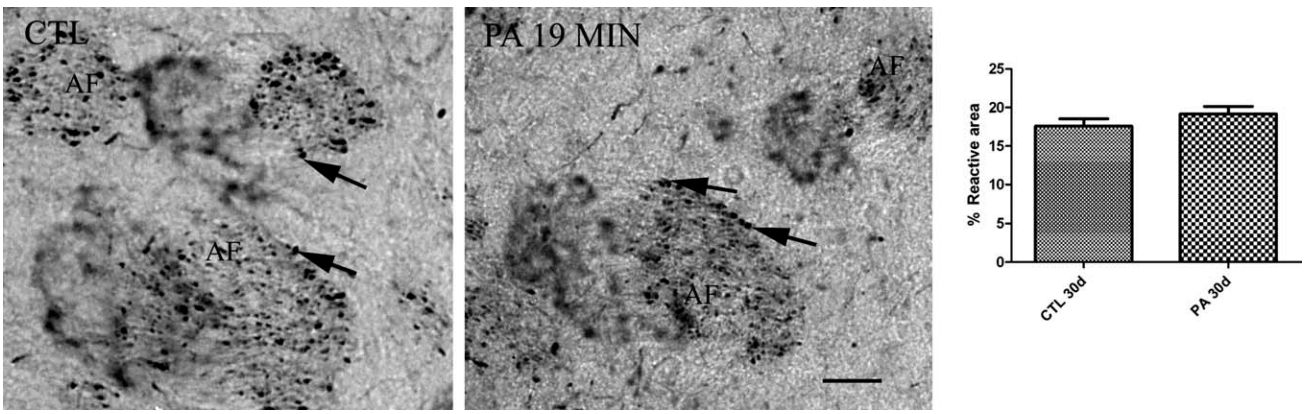


Fig. 6. Optical microscope images of MAP-2 immunostaining from dorsal striatal area. A decrease in the immunostaining was observed in severe PA rats. Scale bar: 10 μm. The assessment of the percentage of reactive area of MAP-2 positive dendrites in striatal sections showed a decrease of the percentage of reactive area of MAP-2 positive dendrites in PA rats in comparison to CTL. AF, axon fascicles. *$P < 0.05$. Bars and error bars represent mean + SEM.

vulnerable to hypoxic-ischemic insults. Calbindin positive cells have been identified as the GABAergic medium spiny neurons projecting to substantia nigra and globus pallidus (DiFiglia et al., 1989; Gerfen et al., 1985; Mallard et al., 1995). Although some reports suggest that calbindin may offer to striatal neurons some protection against moderate excitotoxic and hypoxic-ischemic insults (Burke et al., 1993; Guan et al., 2000), other studies have reported that cell types containing calcium binding proteins are more vulnerable to hypoxia or ischemia (Freund et al., 1990; Guan et al., 2000; Mallard et al., 1995). The results of the present study reveal a neuronal loss in the striatum after one month of PA. Electron microscopy observations and calbinding immunostaining confirmed our data. Consistent with our previous observations (Capani et al., 2009), these findings support the idea that GABAergic neurons are highly vulnerable to PA.

### Modifications on dendritic shaft and axons cytoskeleton after PA

Striatum is associated with the regulation of the motor activity, so the axonal neurofilament impairment could be related to this behavioral deficit (Millerot-Serrurot et al., 2007). PA did not produce differences in the percentage of reactive area of NF-H after 30 days of the injury. These findings could be correlated with the fact that in other areas of the CNS, NFs recovered their normal distribution after some time of the induction of the ischemia (Nakamura et al., 1992). Previous studies have demonstrated a specific increase in NF-200 at six months after PA, suggesting a cellular recovery and adaptative processes that could be attributed to axon regeneration (Cebral et al., 2006; Grady et al., 1993). In addition, these results are in agreement with our previous data (Capani et al., 2009), which shows no

alterations in the presynaptic terminal and myelinic axons at electron microscopy level after six months of PA induction. Consistent with this point of view, we have observed behavioral changes after three months of PA induction (Galeano et al., 2011). Morphological alterations in MAP-2 dendrites are considered a typical change after a hypoxia-ischemia injury and an early marker for neurodegeneration (Lingwood et al., 2003; Saraceno et al., 2010). Previous studies showed that in other areas vulnerable to PA, the percentage of reactive area of MAP-2 also decreases four months after PA (Saraceno et al., 2010). In this study, a slight decrease in the percentage of reactive area of MAP-2 staining was seen in the PA group. Since dynamic microtubules are important to maintain neuronal morphology and function (Kapitein et al., 2011), this decrement in the staining of MAP-2 in dendritic shaft might contribute to the neuronal loss observed in PA animals.

### F-actin cytoskeleton changes after PA

An early increment of glutamate in the extracellular space is observed after a hypoxic-ischemic insult (Choi et al., 1995). This excessive release of glutamate produces a cascade of events in the dendritic spines that leads to cell death (Aon et al., 2010; Capani et al., 2009; Dunah et al., 2003; Endres et al., 1999; Liu et al., 2004, 2006; Li et al., 2007; Martone et al., 1999; Schafer et al., 2009). Structure and function of dendritic spines are dynamically regulated by different cellular pathways acting on the actin cytoskeleton. Using photooxidation with phalloidin-eosin (Capani et al., 2001a,c, 2008; Fukazawa et al., 2003; Ouyang et al., 2005) we were able to study the F-actin cytoskeleton modifications induced by PA. In agreement with previous reports in hippocampal cell culture (Gisselsson et al., 2005), we observed in vivo an increment in the actin staining in dendritic spines after one month of the asphyctic insult. Using electron microscopy we showed that augmentation in the F-actin staining at light confocal level corresponds with the increment in the F-actin positive mushrooms type dendritic spines. Western blot data also confirmed these observations. These types of spines have been involved in memory consolidation (Fukasawa et al., 2003) and protein transportation in dendritic spines (Ouyang et al., 2005). Thus impairment in actin dynamics in mushroom-shaped spines might drive some alterations induced by PA. Consistent with these results, disruption of receptor-scaffold proteins, as NMDA-PSD 95, which depend on actin polymerization interactions, can prevent cell death after ischemia (Aarts et al., 2002).

The actin cytoskeleton is highly regulated by several actin binding proteins (ABP) (Pollard et al., 2003) many of which are involved in the regulation of neuronal death during ischemia and are strongly linked with changes in spine morphology (Endres et al., 1999; Gisselsson et al., 2010; Harms et al., 2004; Yildirim et al., 2008). Since we observed an increment in the polymerized form of actin (F-actin), our data suggest that the modifications of F-actin in the dendritic spines could drive the neuronal and synaptic alterations induced by PA. Thus, alterations in depolymerization/polymerization dynamics in the spine actin cytoskeleton after PA could be involved in the short and long-term diseases induced by PA.

## CONCLUSIONS

Taken together, these data suggest that early changes in the brain induced by PA lead to cytoskeletal modifications of neuronal cytoskeleton. Recently, microtubule plus end has emerged as a regulator of the actin cytoskeleton (Hoogenraad and Akhmanova, 2010). Therefore, the alterations in MAP-2 and actin could be involved in the mechanism of neuronal loss observed after the PA induction. Although further studies will be necessary to determine the key role of cytoskeleton changes, it is tempting to speculate that cytoskeleton alterations might be involved in the generation of an aberrant biochemical pathway that leads into long-term modifications in the brain of PA animals, as we described in a previous article (Capani et al., 2009).

## ACKNOWLEDGMENTS

The authors thank Ing. Elisa María Bocanegra and Ing. Roberto Francisco Domizio from IHEM–CONICET (National University of Cuyo). Gustavo Ezequiel Saraceno, Pablo Galeano and Juan Ignacio Romero are fellowship holders from CONICET (Argentina).

## REFERENCES

Aarts M, Liu Y, Liu L, Besshoh S, Arundine M, Gurd JW, Wang YT, Salter MW, Tymianski M. 2002. Treatment of ischemic brain damage by perturbing NMDA receptor- PSD-95 protein interactions. Science 298:846–850.

Amiel-Tison C, Ellison P. 1986. Birth asphyxia in the fullterm newborn: early assessment and outcome. Dev Med Child Neurol 28:671–682.

Aggoun-Zouaoui D, Margalli I, Borrega F, Represa A, Plotkine M, Ben-Ari Y, Charriaut-Marlangue C. 1998. Ultrastructural morphology of neuronal death following reversible focal ischemia in the rat. Apoptosis 3:133–141.

Aon-Bertolino ML, Romero JI, Galeano P, Holubiec M, Badorrey MS, Saraceno GE, Hanschmann EM, Lillig CH, Capani F. 2011. Thioredoxin and glutaredoxin system proteins-immunolocalization in the rat central nervous system. Biochim Biophys Acta 1810:93–110.

Bjelke B, Andersson K, Ogren SO, Bolme P. 1991. Asphyctic lesion: proliferation of tyrosine hydroxylase-immunoreactive nerve cell bodies in the rat substantia nigra and functional changes in dopamine neurotransmission. Brain Res 543:1–9.

Bottiger BW, Schmitz B, Wiessner C, Vogel P, Hossman KA. 1998. Neuronal stress response and neuronal cell damage after cardiocirculatory arrest in rats. J Cereb Blood Flow Metab 18:1077–1087.

Burke RE, Baimbridge KG. 1993. Relative loss of the striatal striosome compartment defined by calbindin D28k immunostaining

following developmental hypoxic-ischemic injury. Neuroscience 56:305–315.
Capani F, Loidl F, López-Costa JJ, Selvin-Testa A, Saavedra JP. 1997. Ultrastructural changes in nitric oxide synthase immunoreactivity in the brain of rats subjected to perinatal asphyxia: neuroprotective effects of cold treatment. Brain Res 775:11–23.
Capani F, Deerinck TJ, Ellisman MH, Bushong E, Bobik M, Martone ME. 2001a. Phalloidin-eosin followed by photo-oxidation: a novel method for localizing F-actin at the light and electron microscopic levels. J Histochem Cytochem 49:1351–1361.
Capani F, Loidl CF, Aguirre F, Piehl L, Facorro G, Hager A, De Paoli T, Farach H, Pecci-Saavedra J. 2001b. Changes in reactive oxygen species (ROS) production in rat brain during global perinatal asphyxia: an ESR study. Brain Res 914:204–207.
Capani F, Martone ME, Deerinck TJ, Ellisman MH. 2001c. Selective localization of high concentrations of F-actin in subpopulations of dendritic spines in rat central nervous system: a three-dimensional electron microscopic study. J Comp Neurol 435:156–170.
Capani F, Loidl CF, Piehl LL, Facorro G, De Paoli T, Hager A. 2003. Long term production of reactive oxygen species during perinatal asphyxia in the rat central nervous system: effects of hypothermia. Int J Neurosci 113:641–654.
Capani F, Saraceno E, Boti VR, Aon-Bertolino L, Fernández JC, Gato F, Kruse MS, Giraldez L, Ellisman MH, Coirini H. 2008. A tridimensional view of the organization of actin filaments in the central nervous system by use of fluorescent photooxidation. Biocell 32:1–8.
Capani F, Saraceno GE, Botti V, Aon-Bertolino L, de Oliveira DM, Barreto G, Galeano P, Giraldez-Alvarez LD, Coirini H. 2009. Protein ubiquitination in postsynaptic densities after hypoxia in rat striatum is blocked by hypothermia. Exp Neurol 219:404–413.
Cebral E, Capani F, Selvín-Testa A, Funes MR, Coirini H, Loidl CF. 2006. Neostriatal cytoskeleton changes following perinatal asphyxia: effect of hypothermia treatment. Int J Neurosci 116:697–714.
Choi D W. 1995. Calcium: still center-stage in hypoxic-ischemic neuronal death. Trends Neurosci 18:58–60.
Deng V, Matagne V, Banine F, Frerking M, Ohliger P, Budden S, Pevsner J, Dissen GA, Sherman LS, Ojeda SR. 2007. FXYD1 is an MeCP2 target gene overexpressed in the brains of Rett syndrome patients and Mecp2-null mice. Hum Mol Genet 16:640–650.
DiFiglia M, Christakos S, Aronin N. 1989. Ultrastructural localization of immunoreactive calbindin D28K in the rat and monkey basal ganglia including subcellular distribution with colloidal gold labelling. J Comp Neurol 279:653–665.
Dorfman VB, Vega MC, Coirini H. 2006. Age-related changes of the GABA-B receptor in the lumbar spinal cord of male rats and penile erection. Life Sci 78:1529–1534.
Dunah AW, Yasuda RP, Wang YH, Luo J, Davila-Garcia M, Gbadegesin M, Vicini S, Wolfe BB. 1996. Regional and ontogenic expression of the NMDA receptor subunit NR2D protein in rat brain using a subunit-specific antibody. J Neurochem 67:2335–2345.
Dunah AW, Standaert DG. 2003. Subcellular segregation of distinct heteromeric NMDA glutamate receptors in the striatum. J Neurochem 85:935–943.
Endres M, Fink K, Zhu J, Stagliano NE, Bondada V, Geddes JW, Azuma T, Mattson MP, Kwiatkowski DJ, Moskowitz MA. 1999. Neuroprotective effects of gelsolin during murine stroke. J Clin Invest 103:347–354.
Fiala JC, Feinberg M, Popov V, Harris KM. 1998. Synaptogenesis via dendritic filopodia in developing hippocampal area CA1. J Neurosci 18:8900–8911.
Fifkova E, Delay RJ. 1982. Cytoplasmic actin in neuronal processes as a possible mediator of synaptic plasticity. J Cell Biol 95:345–350.
Freund TF, Buzsaki G, Leon A, Baimbridge KG, Somogyi P. 1990. Relationship of neuronal vulnerability and calcium binding protein immunoreactivity in ischemia. Expl Brain Res 83:55–66.
Fukazawa Y, Saitoh Y, Ozawa F, Ohta Y, Mizuno K, Inokuchi K. 2003. Hippocampal LTP is accompanied by enhanced F-actin content within the dendritic spine that is essential for late LTP maintenance in vivo. Neuron 38:447–460.
Galeano P, Blanco Calvo E, Madureira de Oliveira D, Cuenya L, Kamenetzky GV, Mustaca AE, Barreto GE, Giraldez-Alvarez LD, Milei J, Capani F. Long-lasting effects of perinatal asphyxia on exploration, memory and incentive downshift. Int J Dev Neurosci (in press). [Epub ahead of print]
Gerfen CR, Baimbridge KG, Miller JJ. 1985. The neostriatal mosaic: compartmental distribution of calcium binding protein and parvalbumin in the basal ganglia of rat and monkey. Proc Natl Acad Sci USA 82:8780–8784.
Gisselsson LL, Matus A, Wieloch T. 2005. Actin redistribution underlies the sparing effect of mild hypothermia on dendritic spine morphology after in vitro ischemia. J Cereb Blood Flow Metab 25:1346–1355.
Gisselsson L, Toresson H, Ruscher K, Wieloch T. 2010. Rho kinase inhibition protects CA1 cells in organotypic hippocampal slices during in vitro ischemia. Brain Res 1316:92–100.
Grady MS, McLaughlin MR, Christman CW, Valadka AB, Fligner CL, Povlishock JT. 1993. The use of antibodies targeted against the neurofilament subunits for the detection of diffuse axonal injury in humans. J Neuropath Exp Neurol 52:143–152.
Grafstein B, Forman DS. 1980. Intracellular transport in neurons. Physiol Rev 60:1167–1284.
Griffin JW, Watson DF. 1988. Axonal transport in neurological disease. Ann Neurol 23:3–13.
Guan J, Bennet TL, George S, Waldvogel HJ, Faull RL, Gluckman PD, Keunen H, Gunn AJ. 2000. Selective neuroprotective effects with insulin-like growth factor-1 in phenotypic striatal neurons following ischemic brain injury in fetal sheep. Neuroscience 95: 831–839.
Gunn AJ. 2000. Cerebral hypothermia for prevention of brain injury following perinatal asphyxia. Curr Opin Pediatr 12:111–115.
Harms C, Bosel J, Lautenschlager M, Harms U, Braun JS, Hortnagl H, Dirnagl U, Kwiatkowski DJ, Fink K, Endres M. 2004. Neuronal gelsolin prevents apoptosis by enhancing actin depolymerization. Mol Cell Neurosci 25:69–82.
Harris KM, Jensen FE, Tsao B. 1992. Three-dimensional structure of dendritic spines and synapses in rat hippocampus (CA1) at postnatal day 15 and adult ages: implications for the maturation of synaptic physiology and long-term potentiation. J Neurosci 12:2685–2705.
Hill A, Volpe JJ. 1981. Seizures hypoxic—ischemic brain injury and intraventricular hemorrhage in the newborn. Ann Neurol 10:109–121.
Hof PR, Schmitz C. 2000. Current trends in neurostereology—introduction to the special issue "Recent advances in neurostereology". J Chem Neuroanat 20:3–5.
Hoogenraad CC, Akhmanova A. 2010. Dendritic spine plasticity: new regulatory roles of dynamic microtubules. Neuroscientist 16: 650–661.
Hotulainen P, Hoogenraad CC. 2010. Actin in dendritic spines: connecting dynamics to function. J Cell Biol 189:619–629.
Kapitein LC, Yau KW, Gouveia SM, van der Zwan WA, Wulf PS, Keijzer N, Demmers J, Jaworski J, Akhmanova A, Hoogenraad CC. 2011. NMDA Receptor Activation Suppresses Microtubule Growth and Spine Entry. J Neurosci 31:8194–8209.
Laufs U, Gertz K, Huang P, Nickenig G, Bohm M, Dirnagl U, Endres M. 2000. Atorvastatin upregulates type III nitric oxide synthase in thrombocytes decreases platelet activation and protects from cerebral ischemia in normocholesterolemic mice. Stroke 31:2442–2449.
Li D, Shao Z, Vanden Hoek TL, Brorson JR. 2007. Reperfusion accelerates acute neuronal death induced by simulated ischemia. Exp Neurol 206:280–287.
Lingwood BE, Dunster KR, Healy GN, Ward LC, Colditz P. 2003. Cerebral impedance and neurological outcome following a mild or severe hypoxic/ischemic episode in neonatal piglets. Brain Res 969:160–167.
Liu CL, Martone ME, Hu B R. 2004. Protein ubiquitination in postsynaptic densities after transient cerebral ischemia. J Cereb Blood Flow Metab 24:1219–1225.
Liu JJ, Zhao H, Sung JH, Sun GH, Steinberg GK. 2006. Hypothermia blocks ischemic changes in ubiquitin distribution and levels following stroke. Neuroreport 17:1691–1695.
Liu M, Dziennis S, Hurn PD, Alkayed NJ. 2009. Mechanisms of gender-linked ischemic brain injury. Restor Neurol Neurosci 27:163–179.
Loidl CF, Herrera Marschitz M, Andersson K, You ZB, Goiny MO, 'Connor WT, Silveira R, Rawal R, Bjelke B. 1994. Long-term effects of perinatal asphyxia on basal ganglia neurotransmitter systems studied with microdialysis in rat. Neurosci Lett 175:9–12.
Loidl CF, Capani F, Lopez-Costa JJ, Selvin-Testa A, Lopez EM, Goldstein J, Pecci-Saavedra J. 1997. Short-term changes in NADPH-diaphorase reactivity in rat brain following perinatal asphyxia neuroprotective effects of cold treatment. Mol Chem Neuropathol 31:301–316.
Luebke JI, Weaver CM, Rocher AB, Rodriguez A, Crimins JL, Dickstein DL, Wearne SL, Hof PR. 2010. Dendritic vulnerability in neurodegenerative disease: insights from analyses of cortical pyramidal neurons in transgenic mouse models. Brain Struct Funct 214:181–199.
Luo L, Chen H, Zirkin BR. 1996. Are Leydig cell steroidogenic enzymes differentially regulated with aging? J Androl 17:509–515.

Mallard EC, Waldvogel HJ, Williams CE, Faull RL, Gluckman PD. 1995. Repeated asphyxia causes loss of striatal projection neurons in the fetal sheep brain. Neuroscience 65:827–836.

Martone ME, Jones YZ, Young SJ, Ellisman MH, Zivin JA, Hu BR. 1999. Modification of postsynaptic densities after transient cerebral ischemia: a quantitative and three-dimensional ultrastructural study. J Neurosci 19:1988–1997.

Millerot-Serrurot E, Chausset A, Mossiat C, Prigent-Tessier A, Bertrand N, Garnier P, Beley A, Marie C. 2007. Effect of early decrease in the lesion size on late brain tissue loss, synaptophysin expression and functionality after a focal brain lesion in rats. Neurochem Int 50:328–335. Epub 2006 Oct 5.

Morgado-Bernal I. 2011. Learning and memory consolidation: linking molecular and behavioral data. Neuroscience 176:12–19.

Murphy DD, Rueter SM, Trojanowski JQ, Lee VM. 2000. Synucleins are developmentally expressed, and alpha-synuclein regulates the size of the presynaptic vesicular pool in primary hippocampal neurons. J Neurosci 20:3214–3220.

Nakamura M, Araki M, Oguro K, Masuzawa T. 1992. Differential distribution of 68 kDa and 200 kDa neurofilament proteins in gerbil hippocampus and their early distributional changes following transient forebrain ischemia. Exp Brain Res 89:31–39.

Osborne NN, Casson RJ, Wood JP, Chidlow G, Graham M, Melena J. 2004. Retinal ischemia: mechanisms of damage and potential therapeutic strategies. Prog Retin Eye Res 23:91–147.

Ouyang Y, Wong M, Capani F, Rensing N, Lee CS, Liu Q, Neusch C, Martone ME, Wu JY, Yamada K, Ellisman MH, Choi DW. 2005. Transient decrease in F-actin may be necessary for translocation of proteins into dendritic spines. Eur J Neurosci 22: 2995–3005.

Paxinos GP, Watson C. 1986. The rat brain stereotaxic. Sydney: Coordinates Academic Press.

Penzes P, Cahill ME, Jones KA, VanLeeuwen JE, Woolfrey KM. 2011. Dendritic spine pathology in neuropsychiatric disorders. Nat Neurosci 14:285–293.

Pollard TD, Borisy G. 2003. Cellular motility driven by assembly and disassembly of actin filaments. Cell 112:453–465.

Ramon y Cajal S. 1909. Histologie du Systeme Nerveux de l'Homme et des Vertebres. Paris: Maloine.

Saraceno GE, Bertolino ML, Galeano P, Romero JI, Garcia-Segura LM, Capani F. 2010. Estradiol therapy in adulthood reverses glial and neuronal alterations caused by perinatal asphyxia. Exp Neurol 223:615–622.

Schafer DP, Jha S, Liu F, Akella T, McCullough LD, Rasband MN. 2009. Disruption of the axon initial segment cytoskeleton is a new mechanism for neuronal injury. J Neurosci 29:13242–13254.

Schmitz C, Hof PR. 2000. Recommendations for straightforward and rigorous methods of counting neurons based on a computer simulation approach. J Chem Neuroanat 20:93–114.

Shankaran S. 2009. Neonatal encephalopathy: treatment with hypothermia. J Neurotrauma 26:437–443.

Svitkina T, Lin WH, Webb DJ, Yasuda R, Wayman GA, Van Aelst L, Soderling SH. 2011. Regulation of the postsynaptic cytoskeleton: roles in development, plasticity, and disorders. J Neurosci 30:14937–14942.

van Bel F, Groenendaal F. 2008. Long-term pharmacologic neuroprotection after birth asphyxia: where do we stand? Neonatology 94:203–210.

Van de Berg WD, Kwaijtaal M, de Louw AJ, Lissone NP, Schmitz C, Faull RL, Blokland A, Blanco CE, Steinbusch HW. 2003. Impact of perinatal asphyxia on the GABAergic and locomotor system. Neuroscience 117:83–96.

Vannucci RC, Perlman JM. 1997. Interventions for perinatal hypoxic–ischemic encephalopathy. Pediatrics 100:1004–1014.

Wang P, Royer M, Houtz RL. 1995. Affinity purification of ribulose-15-bisphosphate carboxylase/oxygenase large subunit epsilon N-methyltransferase. Protein Expr Purif 6:528–536.

Wang CE, Tydlacka S, Orr AL, Yang SH, Graham RK, Hayden MR, Li S, Chan AW, Li XJ. 2008. Accumulation of N-terminal mutant huntingtin in mouse and monkey models implicated as a pathogenic mechanism in Huntington's disease. Hum Mol Genet 17: 2738–2751.

Weibel HP, Kiessling J. 1978. The effect of noise trauma on speech discrimination in silence and under influence of party noise (author's transl). Arch Otorhinolaryngol 219:413–414.

Yildirim F, Gertz K, Kronenberg G, Harms C, Fink KB, Meisel A, Endres M. 2008. Inhibition of histone deacetylation protects wild-type but not gelsolin-deficient mice from ischemic brain injury. Exp Neurol 210:531–542.